Chemical Science

ROYAL SOCIETY OF CHEMISTRY

EDGE ARTICLE

View Article Online
View Journal | View Issue

Cite this: *Chem. Sci.*, 2023, **14**, 4759

All publication charges for this article have been paid for by the Royal Society of Chemistry

Received 30th January 2023
Accepted 10th March 2023

DOI: 10.1039/d3sc00524k

rsc.li/chemical-science

High-affinity single and double helical pseudofoldaxanes with cationic guests†

Yulong Zhong, ‡[a] Thomas A. Sobiech,‡[a] Brice Kauffmann, [b] Bo Song, [c] Xiaopeng Li, [d] Yann Ferrand,[e] Ivan Huc [f] and Bing Gong *[a]

Two aromatic oligoamides, the 8-residue **H8** and 16-residue **H16**, that adopt stable, cavity-containing helical conformations were examined for their complexation of a rodlike dicationic guest, octyl viologen (OV^{2+}) and *para*-bis(trimethylammonium)benzene (TB^{2+}). Studies based on 1D and 2D ^{1}H NMR, isothermal titration calorimetry (ITC), and X-ray crystallography demonstrated that **H8** and **H16** wraps around two OV^{2+} ions as a double helix and a single helix, respectively, resulting in 2 : 2 and 1 : 2 complexes. Compared to **H8**, the longer **H16** binds the OV^{2+} ions with much higher binding affinity and with extraordinary negative cooperativity. In contrast to its 1 : 2 binding with OV^{2+}, the binding of helix **H16** with the bulkier guest TB^{2+} shows a 1 : 1 ratio. Host **H16** also selectively binds OV^{2+} in the presence of TB^{2+}. This novel host–guest system features pairwise placement of the otherwise strongly repulsive OV^{2+} ions in the same cavity, strong negative cooperativity, and mutual adaptability of hosts and guests. The resultant complexes are highly stable [2]-, [3]-, and [4]pseudo-foldaxanes with few known precedents.

Introduction

A major aim in molecular recognition is the development of structurally and/or functionally tunable hosts capable of tailoring ionic and molecular guests.[1] Since the discovery of crown ethers, a bewildering array of disc-like macrocyclic hosts containing two-dimensional (2D) binding cavities have been created.[2] Hosts such as cryptands,[3] cavitands,[4] and various cages[5] containing deepened cavities are also known to have drastically enhanced binding affinity and selectivity for various guest species.

Tube-like macrocycles such as cyclodextrins,[6] calixarenes,[7] cucurbit[*n*]urils,[8] pillar[*n*]arenes,[9] and other systems[10] provide a class of hosts offering three-dimensional (3D) cavities with legs or walls defining their inner surfaces.[11] Many such hosts, especially those with covalently locked, overall rigid conformations and non-deformable cavities, show spectacular recognition capability. For example, cucurbit[*n*]urils exhibit remarkably tight binding affinities (up to 10^{17} M^{-1} in water) for rigid cationic guests.[12]

Tubular structures with cylindrical cavities of adjustable lengths (or depths) may serve as hosts with unique binding and transport capability, leading to new understanding of host–guest interactions. For example, hosts with deep cavities may accommodate long, rodlike guests and provide fundamental understanding of the role played by multiple non-covalent forces in host–guest binding. Elongated cavities spanning the lipid bilayers can serve as transmembrane channels that facilitate mass transport with selectivity and large flux,[13,14] and allow the identification of guest species without relying on specific guest binding. Several self-assembling organic nanotubes are known.[15–21] The majority of such nanotubes, while showing many interesting binding and transport properties, have undefined length, deformable shapes, and low stability that limit their study and applications. Molecular tubes with non-deformable inner cavities reminiscent of those of carbon nanotubes may be constructed by extending the covalent frameworks of rigid tubular macrocycles such as cucurbit[*n*]urils. Such a possibility, while fascinating, remains to be realized until daunting synthetic challenges are addressed.

A conceptually feasible strategy for constructing molecular tubes is the folding of synthetically accessible oligomers into helices.[22] With helical cavities, such foldamers can serve as hosts for recognizing ionic and neutral guests. Examples of foldamer-based hosts for neutral small molecules were reported by Lehn,[23] Moore,[24] Inouye,[25] Li,[26] Huc,[27] and Jeong;[28] those for recognizing cations were described by Lehn,[29] Chen,[30] Fox,[31] Gong,[32] and

[a]*Department of Chemistry University at Buffalo, The State University of New York Buffalo, New York 14260, USA. E-mail: bgong@buffalo.edu*

[b]*IECB, UAR3033 Univ. Bordeaux, CNRS, IN-SERM 2 rue Robert Escarpit, Pessac, 33600, France*

[c]*Department of Chemistry, Northwestern University Evanston, IL 60208, USA*

[d]*College of Chemistry and Environmental Engineering, Shenzhen University, Shenzhen, Guangdong 518060, China*

[e]*Institut de Chimie et Biologie des Membranes et des Nano-objets, UMR 5248 CNRS, Universite de Bordeaux, F33600 Pessac, France*

[f]*Department Pharmazie, Ludwig-Maximilians-Universität München, D-81377 Munich, Germany*

† Electronic supplementary information (ESI) available: 1D and 2D ^{1}H NMR spectra, ESI-TOF spectra, ITC isotherms and procedures, crystallogenesis and X-ray data. CCDC 2103075 and 2103076. For ESI and crystallographic data in CIF or other electronic format see DOI: https://doi.org/10.1039/d3sc00524k

‡ These authors have contributed equally to this work.

Zeng;[33] and hosts for anions were created by Jeong,[34] Craig,[35] Flood,[36] Guichard,[37] Berryman,[38] and Gong.[39] Except for a few systems,[26,27,32,33] the majority of foldamer hosts known thus far are those undergoing guest-induced folding driven by binding enthalpy. Association constants (K) between such foldamers and guests including ions and small molecules are typically from 10^2 to 10^4 M^{-1} (up to 10^7 M^{-1}) in organic solvents such as chloroform and acetonitrile; and from 10^3 to 10^4 M^{-1} (up to 10^6 M^{-1}) in water-containing solvents with the binding driven by hydrophobic effects. As noncyclic hosts, helical foldamers exhibit unique binding behavior. For example, they can wind around rod-like dumbbell-shaped guests to give host–guest complexes, dubbed by Huc and Ferrand as foldaxanes, that possess properties both similar to and different from traditional rotaxanes.[40]

While a few short foldamers adopting stably folded conformations are known,[26,27,32,33] multi-turn helical foldamers with stable, preorganized cavities capable of binding common organic guests, *i.e.*, those with a size larger than the diameter (~4 Å) of linear alkyl chains,[41] are rare.[42,44,45] One class of foldamers with highly stable helical conformations and a sufficiently large cavity are represented by general structure **H2n** (Fig. 1a, top), which we first proposed and subsequently established.[22] With their backbones being constrained by highly favorable three-center hydrogen bonds,[43] oligoamides **H2n** of different lengths, such as the 8-residue **H8** and the 16-residue **H16** (Fig. 1a), all fold into cavity-containing, "hollow" helices.[44] Oligoamides folding into helices of up to 3 turns were synthesized recently, with the crystal structure of **H16** revealing a compact helix having ~6.6 residues per turn and a non-deformable inner pore that is ~9 Å across.[45] Independent of their lengths, helices **H2n** were found to be stable in solvents of different polarities and at elevated temperatures.[44d] Thus, by synthetically adjusting the length of oligoamides **H2n**, stable hollow helices with tunable but defined lengths and inner cavities of a fixed diameter are obtained. With inward-pointing amide oxygens decorating their inner walls, the cylindrical-shaped cavities of helices **H2n** are highly electronegative and strongly H-bonding, which are distinctly different from the hydrophobic cavities of known high-affinity hosts such as cucurbit[*n*]urils. As molecular tubes with electronegative cavities having multiple preorganized amide oxygen atoms, our hollow helices are expected to strongly bind cationic guests of suitable sizes.

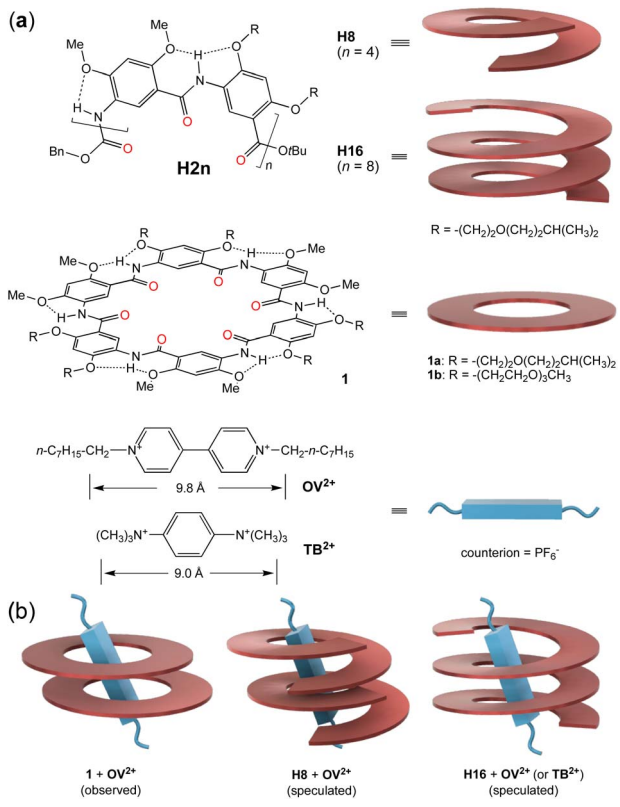

Fig. 1 (a) Structures of aromatic oligoamide **H2n**, macrocycle **1**, and guests OV^{2+} and TB^{2+}. Cartoons on the right illustrate the helical, cyclic, and rodlike shapes of **H8**, **H16**, **1**, and the two cationic guests. (b) Illustrations of the observed 2 : 1 complex between **1** and OV^{2+}, the assumed 2 : 1 complex between **H8** and OV^{2+}, and the 1 : 1 complex between **H16** and OV^{2+} or TB^{2+}.

Sharing the same rigid backbone with oligoamides **H2n**, six-residue macrocycles **1** (Fig. 1a, middle) were found to strongly bind octyl viologen (OV^{2+}) (Fig. 1a, bottom) in their preorganized electronegative cavity in a highly polar solvent like DMSO or DMF.[46] Since the cavity of one molecule of **1** is too "thin" to match the length of the bipyridinium segment of guest OV^{2+}, two molecules of **1** were observed to stack to provide a cavity with a sufficient depth for binding the cationic rod (Fig. 1b, left). The cationic guest threads through the cavities of the two stacked macrocycles, leading to a 2 : 1 complex $\mathbf{1}_2 \cdot OV^{2+}$ with overall association constants (K_{total}) of ~10^{11} M^{-2} in DMSO/$CHCl_3$ (1/1, v/v) and ~10^8 M^{-2} in DMF.

The high affinity of macrocycles **1** for guest OV^{2+} suggests that helical oligoamides **H2n**, with their electronegative cavities, should also strongly bind this and other rodlike cationic guests. To match the bipyridinium rod of guest OV^{2+}, a short (~1 turn) helix needs to stack into a self-assembling host consisting of two or more helical molecules. In contrast, a long helix providing a sufficiently deep cavity that matches the cationic segment will serve as a unimolecular host. Here we show that helical oligoamides **H2n** form extremely stable complexes with OV^{2+} guests to generate [2]-, [3]-, and [4]-pseudofoldaxanes. Binding affinities are so strong that they lead to the unusual stacking of the dicationic guests in the electronegative interior of the helices.

Results and discussion

Design consideration

To probe the possibility of tailoring the size (length) of guests with helical oligoamides **H2n**, oligoamides **H8** and **H16** were studied for their binding with guest OV^{2+}. Based on the 2 : 1 binding of macrocycles **1** with OV^{2+}, oligoamide **H8**, as a helix of ~1.2 turns, was assumed to bind guest OV^{2+} to give a 2 : 1 complex (Fig. 1b, middle). The ~2.5-turn helix **H16** provides a cavity with a depth (~9 Å) that largely matches the length of the bipyridinium segment (~9.8 Å, between the two N^+CH_2-carbons), and was conjectured to bind guest OV^{2+} in a 1 : 1 ratio (Fig. 1b, right). As a unimolecular host, **H16** was expected to bind OV^{2+} with lowered entropic cost and thus higher binding affinity than that between helix **H8** and the same guest. To further demonstrate the role of positive charges

and the bulkiness of the guest in host–guest binding, cationic guest 1,4-bis(trimethylammonium)benzene ($\mathbf{TB}^{2+}$) (Fig. 1a, bottom), with a length (~9.0 Å, between the hydrogens of the two $N^{+}(CH_3)_3$ groups) that is the same as the depth of the cavity of helix **H16**, is designed and examined for its interaction with **H16**. Consistent with our expectation, our studies demonstrate that helix **H8** assembles into dimeric (double helical) host $\mathbf{(H8)_2}$ for guests $\mathbf{OV}^{2+}$, while helix **H16** serves as a unimolecular host for guests $\mathbf{OV}^{2+}$ and $\mathbf{TB}^{2+}$. Surprisingly, the interiors of double helix $\mathbf{(H8)_2}$ and helix **H16** are able to accommodate two otherwise highly repulsive $\mathbf{OV}^{2+}$ ions.

Binding process and stoichiometry

The host–guest interactions between oligoamides **H8** or **H16** and $\mathbf{OV}^{2+}$ were first probed with ^{1}H NMR titration experiments. Since the ^{1}H-NMR signals of **H8** or **H16** and its complex(es) with $\mathbf{OV}^{2+}$ are broadened at room temperature, this prevents the assignment of the ^{1}H NMR resonances and hampers 2D NMR studies. ^{1}H NMR studies were performed at 45 °C at which the ^{1}H NMR signals turn sharp, allowing all signals to be properly assigned. In DMSO-d_6/$CDCl_3$ (3/7, v/v), titrating **H8** with 0 to 2 equiv. of $\mathbf{OV}^{2+}$ resulted in a downfield shift of the resonances of aromatic protons b1 (Fig. S1†), b2 through b7 of **H8**, and protons α and β of $\mathbf{OV}^{2+}$ (Fig. 2a), along with the upfield shift of the signal of proton b8 (Fig. 2a). Among the signals of aromatic protons b2 through b8, those of protons b3, b5, b7, and b8 remained well dispersed with an increasing proportion of $\mathbf{OV}^{2+}$ (Fig. 2a). With more than one equivalent of $\mathbf{OV}^{2+}$, the resonances of aromatic protons b2 through b8 (Fig. 2a) show insignificant shifts, while the signals of protons α and β of $\mathbf{OV}^{2+}$ continue to move upfield, approaching those of a free $\mathbf{OV}^{2+}$ ion with increasing proportions of the guest.

Plotting the chemical shifts of protons b3, b5, b7, and b8 of **H8** against the ratio of $\mathbf{OV}^{2+}$ reveals a linear dependence that changes abruptly at one equiv. of $\mathbf{OV}^{2+}$ (Fig. 2b), indicating that **H8** and $\mathbf{OV}^{2+}$ bind in a 1 : 1 ratio that is corroborated by a Job plot (Fig. 2c). The observation of only one set of ^{1}H NMR signals with varying proportions of $\mathbf{OV}^{2+}$ suggests that the free and bound host and guest undergo rapid exchange on the ^{1}H NMR time scale. Since the ^{1}H resonances of **H8** exhibit an insignificant shift with ≥1 equiv. of $\mathbf{OV}^{2+}$, the equilibrium must have shifted toward the presumable 1 : 1 complex as the dominant species.

Titrating **H16** with $\mathbf{OV}^{2+}$ led to significant changes in the aromatic and amide region from 5.9 to 10.4 ppm (Fig. 3). With <1 equiv. of $\mathbf{OV}^{2+}$, the region containing the resonances of internal aromatic protons b1 through b16 is found to contain many (~32 aromatic Hs) signals that indicate the presence of free **H16** and the 1 : 1 complex of **H16** and $\mathbf{OV}^{2+}$ in slow exchange. With 1 equiv. of $\mathbf{OV}^{2+}$, only the 16 new signals attributed to the 1 : 1 complex remain. With more than one but less than two equiv. of $\mathbf{OV}^{2+}$, the 16 peaks attributed to the 1 : 1 complex and another set of ~16 new peaks corresponding to the 1 : 2 complex are found in this region, indicating that the 1 : 1 and 1 : 2 complexes are in slow exchange; with >2 equiv. of $\mathbf{OV}^{2+}$, the second set of 16 new peaks remain and the peaks of the 1 : 1 complex completely disappear, suggesting the presence of only the 1 : 2 complex of **H16** and $\mathbf{OV}^{2+}$. In addition, the signals of protons α and β belonging to free $\mathbf{OV}^{2+}$ at 9.4 and 8.7 ppm are observed with >2 equiv. of $\mathbf{OV}^{2+}$. These observations indicate that the binding of **H16** with $\mathbf{OV}^{2+}$ happens stepwise. The formation of the 1 : 1 complex occurs first as up to 1 equiv. of $\mathbf{OV}^{2+}$ is added, followed by the appearance of the 1 : 2 complex with ≥1

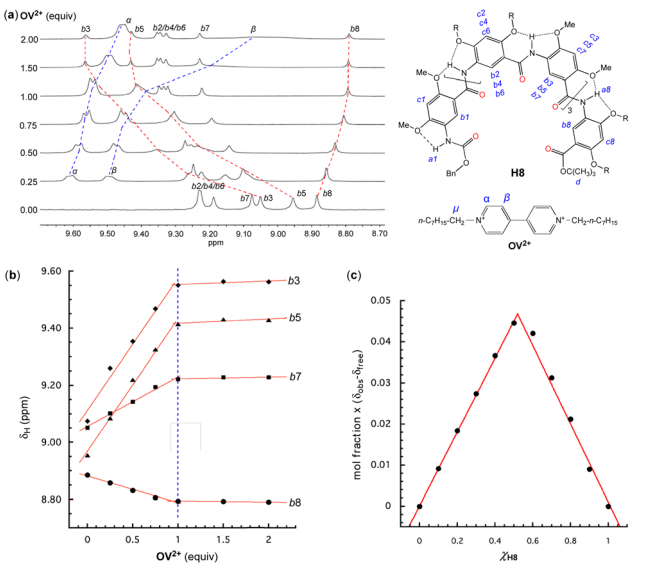

Fig. 2 Oligoamide **H8** (1 mM) titrated with 0 to 2 equiv. of guest $\mathbf{OV}^{2+}\cdot(\mathbf{PF_6}^-)_2$ in DMSO-d_6/$CDCl_3$ (3/7, v/v) at 45 °C. (a) ^{1}H NMR spectra (400 MHz), (b) changes in chemical shifts (δ_H) of aromatic protons b3, b5, b7, and b8 of **H8** *vs.* the equiv. of $\mathbf{OV}^{2+}\cdot(\mathbf{PF_6}^-)_2$ and, (c) Job's plot based on the chemical shifts of proton b8 of **H8** in the presence of different ratios of $\mathbf{OV}^{2+}\cdot(\mathbf{PF_6}^-)_2$. The assignment of ^{1}H resonances was assisted with 2D (NOESY) spectra.

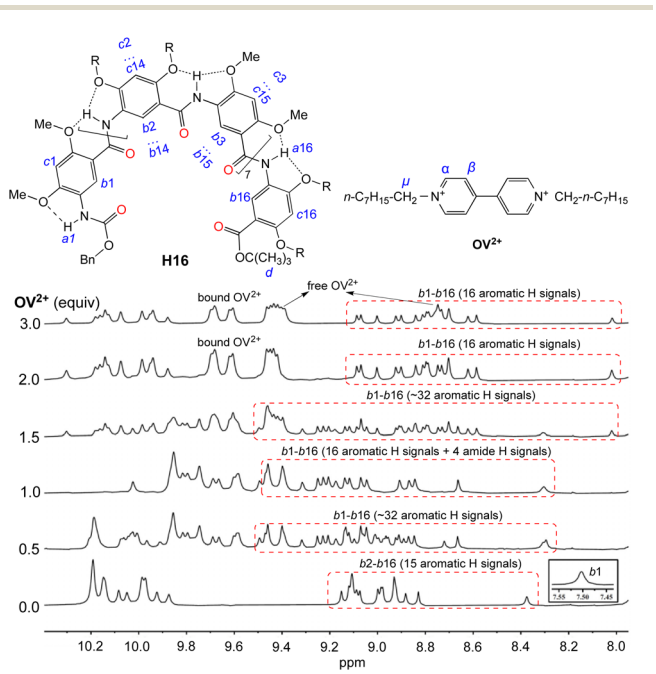

Fig. 3 ^{1}H NMR spectra of **H16** (1 mM) titrated with 0 to 3 equiv. of $\mathbf{OV}^{2+}\cdot(\mathbf{PF_6}^-)_2$ in DMSO-d_6/$CDCl_3$ (2/3, v/v) at 45 °C. The assignment of ^{1}H resonances was assisted with 2D (NOESY) spectra.

equiv. of OV^{2+}. The presence of ≥2 equiv. of OV^{2+} completely drives the equilibrium toward the side of the 1 : 2 complex. In the presence of >2 equiv. of OV^{2+}, the unchanged signals of **H16** and the simultaneous presence of both the free and bound OV^{2+} suggest that **H16** strongly binds OV^{2+}, with the free and bound OV^{2+} undergoing no or slow exchange on the NMR time scale.

To provide additional evidence for the binding stoichiometry between **H8** or **H16** with OV^{2+}, mixtures of **H8** or **H16** and guest OV^{2+} in different ratios were examined with electrospray-ionization quadrupole time-of-flight mass spectrometry (ESI-QTOF). The mass spectrum of the 2 : 1 mixture of **H8** and OV^{2+} contains two peaks given by the 2 : 1 complex $(\mathbf{H8})_2\cdot OV^{2+}$, along with a third peak corresponding to the 1 : 1 complex $\mathbf{H8}\cdot OV^{2+}$ (Fig. S2a†). The mass spectrum of the 1 : 1 mixture of **H8** and OV^{2+} (Fig. S2b†) reveals a major peak for $\mathbf{H8}\cdot OV^{2+}$, the 1 : 1 complex, and another peak of $(\mathbf{H8})_2\cdot OV^{2+}$, the 2 : 1 complex. Surprisingly, a peak corresponding to $(\mathbf{H8})_2\cdot(OV^{2+})_2$, the 2 : 2 complex, which cannot be distinguished from the 1 : 1 complex by NMR, is also observed. In the spectrum of the 1 : 2 mixture of **H8** and OV^{2+} (Fig. S2c†), the ions of the 1 : 1 complex $\mathbf{H8}\cdot OV^{2+}$ (dominant), 2 : 1 complex $(\mathbf{H8})_2\cdot OV^{2+}$ (much weaker), and 2 : 2 complex $(\mathbf{H8})_2\cdot(OV^{2+})_2$ are detected. In contrast, the 1 : 2 complex $\mathbf{H8}\cdot(OV^{2+})_2$ could not be clearly detected in the spectra of the mixtures. These observations suggest that **H8** can bind with OV^{2+} in both 1 : 1 and 2 : 2 ratios. Complex $(\mathbf{H8})_2\cdot OV^{2+}$, which was observed in the mass spectra of all three mixtures, seems to be the intermediate between the 1 : 1 and 2 : 2 complexes.

The ESI-QTOF spectrum of the 1 : 1 mixture of **H16** and OV^{2+} reveals the presence of only the 1 : 1 complex $\mathbf{H16}\cdot OV^{2+}$ (Fig. S3a†). With the proportion of OV^{2+} being doubled, the 1 : 2 mixture of **H16** and OV^{2+} gives a mass spectrum containing peaks of both the 1 : 1 complex $\mathbf{H16}\cdot OV^{2+}$ and 1 : 2 complex $\mathbf{H16}\cdot(OV^{2+})_2$ (Fig. S3b†), which suggests that increasing the ratio of OV^{2+} drives the complexation of the second guest OV^{2+} into the cavity of **H16**.

The results from studies mainly based on mass spectrometry and confirmed by single crystal structures (see Fig. 5 below) indicate that the originally expected complexation stoichiometry and processes of **H8** and **H16** with OV^{2+} shown in Fig. 1 need to be revised. As shown in Fig. 4a, the complexation of **H8** for OV^{2+} involves the initial formation of the 1 : 1 complex, followed by the binding of the second molecule of **H8** to give the 2 : 1 complex which, by binding the second OV^{2+}, yields the 2 : 2 complex (Fig. 4a). The 1 : 1, 2 : 1, and 2 : 2 complexes of **H8** and OV^{2+} undergo rapid exchange as shown by the observation of only one set of signals throughout the ^{1}H NMR titration (Fig. 2a), making it impossible to distinguish the complexes detected by ESI-TQF in solution. Thus, the major species in solution might be the 1 : 1 complex, a possibility that is not supported by evidence from mass spectrometry and X-ray structure, which clearly indicate the presence of the 2 : 2 complex.

In solution, the formation of the $(\mathbf{H8}:OV^{2+})$ 2 : 1 complex from the binding of the 1 : 1 complex with another molecule of **H8** is very likely accompanied by positive cooperativity that is promoted by the favorable stacking interactions between the two molecules of **H8**, along with additional C–H···O interactions in the 2 : 1 complex $(\mathbf{H8})_2\cdot OV^{2+}$. Such favorable (positive) binding

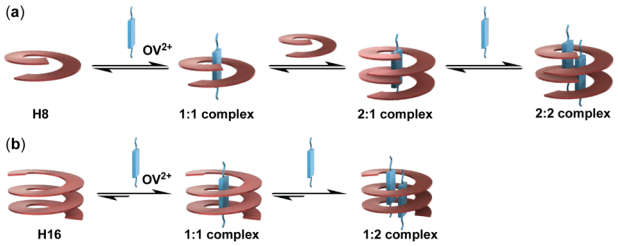

Fig. 4 Schematic illustrations of the complexation processes of (a) oligoamide **H8** and (b) oligoamide **H16** with guest OV^{2+}.

cooperativity was directly observed in the binding of macrocycle **1** (Fig. 1), which shares the same aromatic backbone with **H8** or **H16**, with OV^{2+}. However, one OV^{2+} could only interact with about half of the binding sites (amide carbonyls) in the cavity of **H8** or its dimer, which would lead to ineffective binding interaction. Binding the second OV^{2+} ion to the 2 : 1 complex $(\mathbf{H8})_2\cdot OV^{2+}$ to give the 2 : 2 complex should be a negative cooperative process due to the repulsion resulted from stuffing two OV^{2+} ions into the cavity of the **H8** dimer. This unfavorable, negative cooperative process offsets the favorable electrostatic and C–H···O interactions the OV^{2+} ions experienced in the electronegative, strongly H-bonding cavity of the **H8** dimer, something that is also exhibited by **H16**. Based on these considerations, in solution, the 2 : 2 complex is more likely to be the major species.

The binding of **H16** with OV^{2+} follows a clear stepwise path, with the 1 : 1 and 1 : 2 complexes, and the unbound **H16** and OV^{2+} undergoing slow exchange (Fig. 4b). The 1 : 1 complex exists as the only host–guest species with up to 1 equiv. of OV^{2+}, and the 1 : 2 complex as the only complex with >2 equiv. of OV^{2+}.

Binding strength and thermodynamic parameters

The binding of OV^{2+} with **H8** and **H16** was then probed with isothermal titration calorimetry (ITC) which, in addition to determining the association constants (K), also provides the corresponding thermodynamic parameters including changes of enthalpy (ΔH), entropy (ΔS), and free energy (ΔG) as shown in Table 1. In MeOH/$CHCl_3$ (3/7, v/v) at 35 °C, the ITC thermogram (Fig. S4a(i)†) for the binding of **H8** with OV^{2+} is consistent with a 1 : 1 binding ratio, with an association constant over 10^6 M^{-1} that reflects both the 1 : 1 and 2 : 2 binding modes. In the same solvent, the complexation of **H16** for OV^{2+} gives an association constant (K_1) over 10^8 M^{-1} for the first binding event, followed by that (K_2) of the second binding event that is three orders of magnitude smaller than K_1 (Fig. S4b†). The high affinity of the first binding event approaches the upper limit of ITC measurements, leading to K_1 with a significant error. In the more polar DMSO/$CHCl_3$ (1/1, v/v) at 45 °C, the binding of **H8** with OV^{2+} gives an apparent association constant of ~10^5 M^{-1} (Fig. S4(ii)†), while the affinities of **H16** and OV^{2+} are also reduced (Fig. S5†), with K_1 over 10^7 M^{-1} and K_2 over 10^4 M^{-1} that are in the range allowing accurate ITC measurements.

For the complexation of **H16** and OV^{2+}, the much stronger first binding step compared to the second step precluded the determination of the binding parameters with one ITC titration. Instead, in DMSO/$CHCl_3$ (1/1), K_1, along with ΔS_1 and ΔH_1, was

Table 1 Association constants, thermodynamic parameters and interaction factors (α), for the complexation of hosts **H8** and **H16** toward guests OV^{2+} and TB^{2+} obtained from ITC experiments

Host	Guest	Solvent	Temp. (°C)	$-\Delta H$ (kcal mol^{-1})	$T\Delta S$ (kcal mol^{-1})	K (or K_1, K_2) (M^{-1})	K_{total}[b] (M^{-2})	α[a]
H8	OV^{2+}	MeOH/$CHCl_3$, (3/7, v/v)	35	8.2 ± 0.1	1.3 ± 0.1	$(5.5 \pm 1.0) \times 10^6$	—	—
H16	OV^{2+}	MeOH/$CHCl_3$, (3/7, v/v)	35	2.7 ± 0.1 (ΔH_1)	9.4 ± 0.4 (ΔS_1)	$(3.6 \pm 2.0) \times 10^8$ (K_1)	$(1.7 \pm 1.1) \times 10^{14}$	0.005
				6.1 ± 0.1 (ΔH_2)	1.9 ± 0.1 (ΔS_2)	$(4.6 \pm 0.3) \times 10^5$ (K_2)		
H8	OV^{2+}	DMSO/$CHCl_3$, (1/1, v/v)	45	1.9 ± 0.1	5.3 ± 0.1	$(1.0 \pm 0.1) \times 10^5$	—	—
H16	OV^{2+}	DMSO/$CHCl_3$, (1/1, v/v)	45	9.1 ± 0.1 (ΔH_1)	1.8 ± 0.2 (ΔS_1)	$(3.2 \pm 0.6) \times 10^7$ (K_1)	$(5.2 \pm 1.9) \times 10^{11}$	0.002
				4.6 ± 0.1 (ΔH_2)	1.6 ± 0.1 (ΔS_1)	$(1.6 \pm 0.3) \times 10^4$ (K_2)		
H16	TB^{2+}	DMSO/$CHCl_3$, (1/1, v/v)	45	13.0 ± 0.1	1.9 ± 0.5	$(3.2 \pm 0.8) \times 10^7$	—	—

[a] Interaction factor $\alpha = 4K_2/K_1$. ($\alpha > 1$: positive cooperativity; $\alpha < 1$: negative cooperativity; $\alpha = 1$ no cooperativity). [b] $K_{total} = K_1 \times K_2$.

obtained by first titrating **H16** (50 μM) with $OV^{2+}\cdot PF_6^-$ (0.5 mM) (Fig. S5a†); the much smaller K_2, along with ΔS_2 and ΔH_2, was obtained by titrating the 1 : 1 mixture of **H16** (3 mM) and $OV^{2+}\cdot PF_6^-$ (3 mM) with $OV^{2+}\cdot PF_6^-$ (30 mM) (Fig. S5b†). The binding of **H16** for OV^{2+}, with its second binding event being three orders of magnitude weaker than the first one, gives interaction factors α (ref. [47]) of 0.005 in MeOH/$CHCl_3$ (3/7) and 0.002 in DMSO/$CHCl_3$ (1/1). Such remarkable negative cooperativity[47] reflects the unfavorable stuffing of the second OV^{2+} guest into the cavity of **H16**. These observations demonstrate that the inner cavity of **H16** offers a highly electronegative environment that not only overcomes the repulsion between the two cationic guests but also provides additional driving force for the formation of the 1 : 2 complex.

In MeOH/$CHCl_3$ (3/7), the first binding event of **H16** and OV^{2+} is entropically driven, which reflects the desolvation of, *i.e.*, the release of methanol molecules from the cavity of **H16** upon binding the first OV^{2+}. The second binding event is enthalpically driven, due to the electrostatic attraction that drives the binding of the second OV^{2+} to the desolvated cavity. In contrast, in DMSO/$CHCl_3$ (1/1), both first and second binding events of **H16** and OV^{2+} are enthalpically driven. As an aprotic solvent, DMSO is not able to effectively solvate the electronegative cavity of **H16**. The poorly solvated cavity of **H16**, with multiple amide carbonyl groups as preorganized binding sites, is amenable to accommodating the cationic guest *via* attractive electrostatic interaction.

The dominant role played by electrostatic interaction is verified by the binding of rodlike guest TB^{2+} which, like guest OV^{2+}, is rigid and carries two positive charges. ITC shows that (Fig. S6†) in DMSO/$CHCl_3$ (1/1), the 1 : 1 binding of **H16** and TB^{2+}, with an association constant (K) over 10^7 M^{-1} that is the same as that of binding the first OV^{2+} with **H16**, is driven predominantly by a favorable (negative) enthalpy change that results from the strong electrostatic interaction between the two positive charges of guest TB^{2+} and the negative cavity of **H16** (Table 1). Unlike the pairwise binding of OV^{2+}, the binding of a second TB^{2+} ion with **H16** was not observed. The bulkiness of the two trimethylammonium groups and the small aromatic surface of TB^{2+} are the most likely reasons that hinder the cramming of two guests TB^{2+} inside the cavity of H16. Thus, by performing structural tuning on the guest, the binding stoichiometry involving host H16 can be adjusted and controlled.

Binding selectivity probed with ^{1}H NMR competition experiments

To examine the binding selectivity of **H16**, the binding of **H16** to OV^{2+} in the presence of TB^{2+} and *vice versa* was compared with ^{1}H NMR titration experiments performed in DMSO-d_6/$CDCl_3$ (2/3, v/v) at 45 °C. Titrating the 1 : 2 mixture of **H16** and $OV^{2+}(PF^{6-})_2$ with 0–1.0 equiv. of $TB^{2+}(PF^{6-})_2$ failed to change the position of the bound OV^{2+} ions, with the signal of aromatic protons of TB^{2+} remaining the same as that of the free (unbound) TB^{2+} ion (Fig. S7a†). In contrast, titrating the 1 : 1 mixture of **H16** and $TB^{2+}(PF^{6-})_2$ with 0–3.0 equiv. of $OV^{2+}(PF^{6-})_2$ led to an upfield shift of the aromatic proton signal of TB^{2+} (Fig. S7b†). With 2 equiv. of $OV^{2+}(PF^{6-})_2$, the signal of the TB^{2+} ion is very close to the position of the signal given by the free TB^{2+} ion. With 3 equiv. of $OV^{2+}(PF^{6-})_2$, the signal of the TB^{2+} ion is at the same position of that of the free TB^{2+} ion. These observations suggest that between OV^{2+} and TB^{2+}, **H16** shows a clear preference for the former despite the higher entropic cost for binding two OV^{2+} ions than binding one TB^{2+} ion.

Crystal structures of complexes $(H8)_2\cdot(OV^{2+})_2$ and $H16\cdot(OV^{2+})_2$

Single crystals of the complexes of OV^{2+} with **H8** and **H16** were obtained *via* liquid–liquid diffusion of methanol into a dichloromethane solution in an NMR tube, which revealed the existence of the 2 : 2 complex $(H8)_2\cdot(OV^{2+})_2$ and 1 : 2 complex $H16\cdot(OV^{2+})_2$ in the solid state, consistent with solution data. The structure of complex $(H8)_2\cdot(OV^{2+})_2$ shows that the two molecules of **H8** form a double helix in which the two helical strands pair in an antiparallel orientation, *i.e.*, the N end of one strand aligns with the C end of the other strand, with the C ends of the two **H8** molecules being placed in the middle of the double helix. In each helix, the phenyl ring of the terminal benzyl group engages in intramolecular edge-to-face interaction with the oligomide backbone.

The bipyridinium segments of the two OV^{2+} ions bind to the cavity of the double helix (Fig. 5a, top) and engage in C–H···O interactions involving 14 of the 16 aromatic C–H groups of the two OV^{2+} ions and the amide carbonyls of **H8**, with an average H···O distance of 2.45 Å. N^+···O distances of 3.02, 3.20, 3.65, and 3.98 Å are found between each of the pyridinium N^+ atoms and its nearest amide carbonyl oxygen of **H8**, indicative of strong charge–dipole interactions. To reduce the repulsion between the two OV^{2+} ions, the two bipyridinium segments in the cavity of the double helix

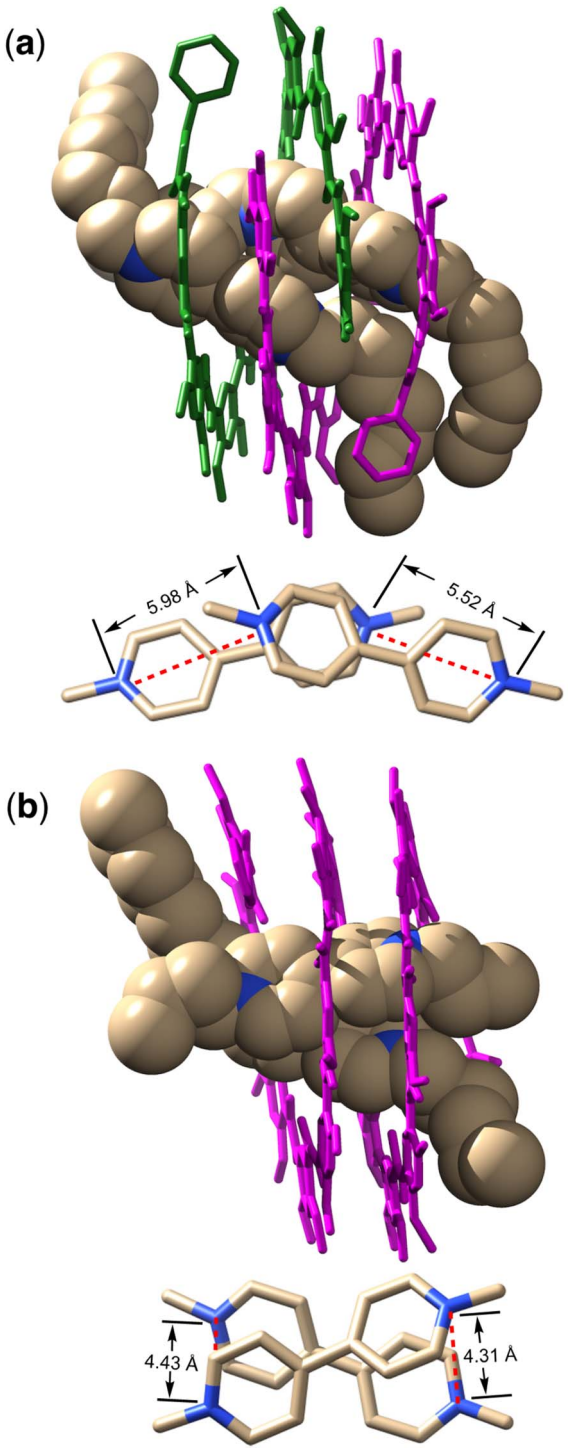

Fig. 5 Crystal structures of (a) complex $(H8)_2\cdot(OV^{2+})_2$ (top), along with the two OV^{2+} ions in the cavity of the double helix of **H8** (bottom) and, (b) complex $H16\cdot(OV^{2+})_2$ (top), along with the two OV^{2+} ions in the cavity of helix **H16** (bottom). The $N^+\cdots N^+$ distances between the termini of the two OV^{2+} ions in each complex are highlighted with red dashed lines. For clarity, all side chains are replaced with methyl groups; the PF_6^- counterions and included solvent molecules are omitted.

align in an offset way, with their long axes crossing over one another with an angle of ~27° and the $N^+\cdots N^+$ distances between the ends of the two bipyridinium units being 5.52 Å and 5.98 Å (Fig. 5a, bottom). Two of the four pyridinium rings of the OV^{2+} ions face each other with an average distance of ~4.3 Å, indicative of very weak, if any, stacking interaction.

Although double helices have been found in a number of other oligoamides,[48] the formation of a double helix shown with oligoamide **H8** is the first example for this series of oligoamides. The capability of oligoamides **H2n** to assemble in such a way was unknown, which indicates the possibly similar behavior in the absence or presence of guests.

Similar to that of OV^{2+} with **H8**, the binding of OV^{2+} to the cavity of **H16** is driven by C–H···O interactions involving 14 of the 16 aromatic CH groups of the OV^{2+} ions and the amide carbonyls of **H16**, with an average H···O distance of 2.39 Å that is shorter than that (2.45 Å) in complex $(H8)_2\cdot(OV^{2+})_2$ (Fig. 5b, top). $N^+\cdots O$ distances of 2.97, 3.10, 3.12, and 4.30 Å, which are overall shorter than those in complex $(H8)_2\cdot(OV^{2+})_2$, are found between each of the pyridinium N^+ atoms and its nearest amide carbonyl oxygen of **H16**, indicative of charge–dipole interactions that are stronger than those in complex $(H8)_2\cdot(OV^{2+})_2$. Unlike the offset alignment of the bipyridinium segments of the two OV^{2+} ions in the cavity of double helix $(H8)_2$, the bipyridinium segments in the cavity of **H16** slide much less along their long axes and show a larger extent of overlap. The two aligned cationic rods have their four aromatic rings being partially stacked with an average stacking distance of 4.0 Å, indicating weak but noticeable stacking interaction (Fig. 5b, bottom). To avoid the N^+ atoms directly facing one another, the bipyridinium segments cross over one another, with an angle of ~42° between their long axes. The $N^+\cdots N^+$ distances of 4.31 and 4.43 Å between the ends of the two bipyridinium units are much shorter than those than in complex $(H8)_2\cdot(OV^{2+})_2$. This arrangement would explain the negative cooperativity between the first and second OV^{2+} binding events.

The crystal structures of complexes $(H8)_2\cdot(OV^{2+})_2$ and $H16\cdot(OV^{2+})_2$ reveal that the two guests OV^{2+} in each complex adjust their alignment to optimize their interaction with each host. Compared to that in complexes $(H8)_2\cdot(OV^{2+})_2$, the cationic segments of OV^{2+} ions in complex $H16\cdot(OV^{2+})_2$, being confined in the more compact cavity of **H16**, have their ends being placed more closely as shown by shorter $N^+\cdots N^+$ distances, leading to a quadruply charged, shorter dimer that engages in stronger interactions with the host as shown by the shorter C–H···O and $N^+\cdots O$ distances. Additional insights into this unique host–guest system are gained by comparing the crystal structure of **H16** alone[45] with that in complex $H16\cdot(OV^{2+})_2$, which indicates that the helical host fine-tunes its folded structure upon binding OV^{2+}. Compared to the ~9 Å diameter of the cavity of helix **H16** alone,[45] the cavity diameter of helix **H16** in complex $H16\cdot(OV^{2+})_2$ increases to over 9.5 Å, presumably to better match the size of the bound OV^{2+} dimer. Such host–guest mutual adaption is made possible by the self-assembling nature of the dimeric guest and the limited conformational flexibility of the host, leading to enhanced host–guest interaction shown by the high binding affinities of **H16** for OV^{2+} and TB^{2+}.

Thus, by overcoming the otherwise strong electrostatic repulsion between guests OV^{2+}, the electronegative cavities of double

helix $(\mathbf{H8})_2$ and helix **H16** are able to bind a pair of guest $\mathbf{OV}^{2+}$ in high affinity. The pairwise binding of the dicationic guests shown by **H8** and **H16** is precedented by few known host–guest systems. In fact, few hosts are known to allow two or more viologen-based guests, *i.e.*, four or more positive charges, to be placed in close proximity in the same cavity. Cucurbit[8]uril (CB[8]), although having a cavity large enough to accommodate two molecules or ions with sizes comparable to that of the bipyridinium segment of viologens, was reported to form a 1 : 1 complex with methyl viologen ($\mathbf{MV}^{2+}$). The complexation of one CB[8] for two $\mathbf{MV}^{2+}$ ions and similar guests has not been realized, presumably because of the strong electrostatic repulsion between the two dicationic guests in the cavity.[49] To the best of our knowledge, the only known 1 : 2 complexes having a dimer of a viologen-based guest residing in the cavity of a host were reported by Chen *et al.*[50] With the binding affinities being presented as "average association constants" (K_{av}) of $\sim 10^3$ M^{-1} in $CD_3CN/CDCl_3$ (1/1, v/v), these 1 : 2 complexes involve a host based on a triptycene-based macrotricycle that provides a partially rigid binding cavity deeper than those of common macrocycles. The guests are viologens carrying β-hydroxyethyl or γ-hydroxypropyl end chains. In this system, the terminal hydroxyl groups of these guests seemed to play a critical role in driving the formation of the 1 : 2 complex since other guests based on dialkyl viologens could only form 1 : 1 complexes with this host.

Solution structures of the complexes probed with two-dimensional NMR spectroscopy

As revealed by 1D ^{1}H NMR spectroscopy, ITC measurements, and X-ray crystallography, the binding of guest $\mathbf{OV}^{2+}$ with oligoamides **H8** and **H16** leads to 2 : 2 complex $(\mathbf{H8})_2\cdot(\mathbf{OV}^{2+})_2$ and 1 : 2 complex $\mathbf{H16}\cdot(\mathbf{OV}^{2+})_2$, respectively. With the assignment of 1D ^{1}H NMR spectra being assisted by COSY and NOESY spectra, the solution structures of these complexes were revealed with two-dimensional (NOESY) ^{1}H NMR experiments.

Fig. 6 shows the partial NOESY spectra of **H8** and $\mathbf{OV}^{2+}$ (1 : 1) recorded in DMSO-d_6/$CDCl_3$ (7/3, v/v) at 45 °C. Strong NOEs between aromatic protons b2 through b8 of **H8** and aromatic protons α and β (Fig. 6a), and methylene protons μ (Fig. 6b) of $\mathbf{OV}^{2+}$, are revealed. NOEs between protons b1 and α, β, and μ are also detected (Fig. S8†). In contrast, no NOE is observed between protons α, β, or μ of $\mathbf{OV}^{2+}$ and aromatic protons c1–c8, *i.e.*, the "exterior" protons of **H8**. These observations demonstrate that the $\mathbf{OV}^{2+}$ ions reside in the cavity of the double helix. A NOE between protons d of **H8** and proton b2 confirms that **H8** remains folded when binding guests $\mathbf{OV}^{2+}$ (Fig. 6c). Another NOE involving protons d and β is also noticed (Fig. 6c), while no NOE can be found between protons d and α, which suggests that the two molecules of **H8** have their C-termini placed in the interior and their N-termini located at the two ends of double helix $(\mathbf{H8})_2$. This observation is consistent with what is revealed by the crystal structure of complex $(\mathbf{H8})_2\cdot(\mathbf{OV}^{2+})_2$, *i.e.*, in solution, the two molecules of **H8** constitute a double helix with an average C_2 symmetry in which the C-terminal residues are placed near each other (Fig. 6d).

The backbone of **H16** follows an N-to-C direction, leading to an unsymmetrical cavity for helix **H16**. Upon binding with **H16**,

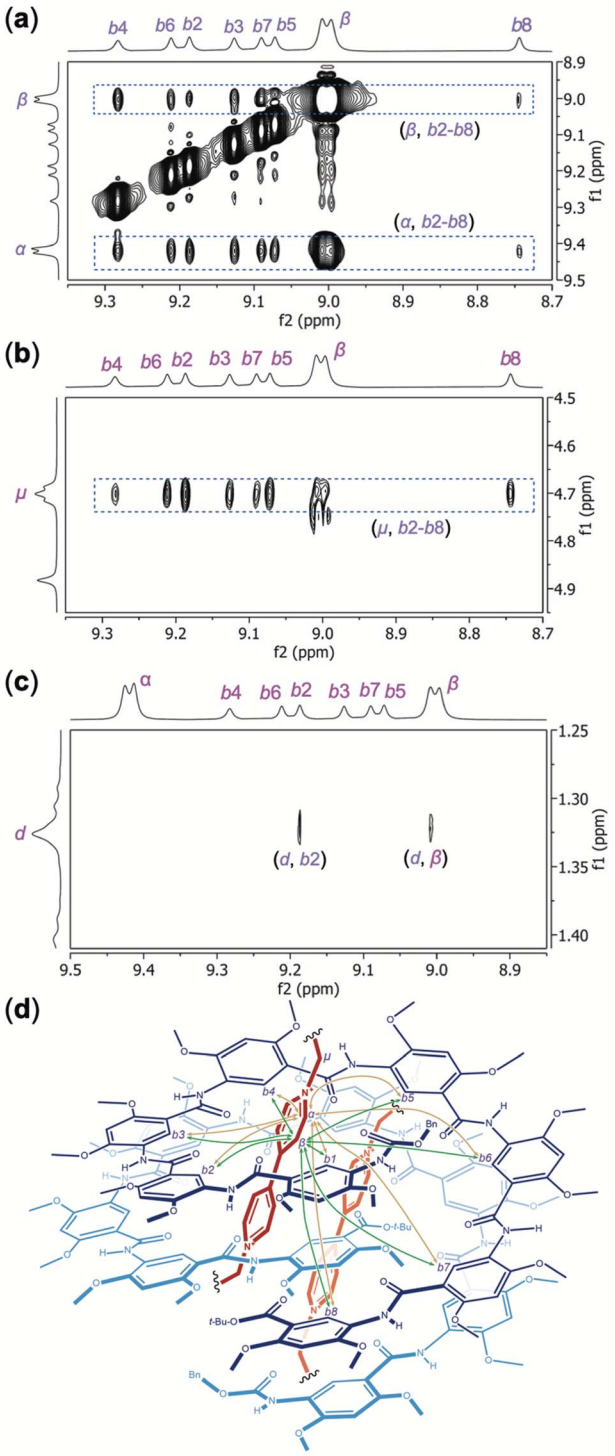

Fig. 6 Partial NOESY spectra (500 MHz, mix time: 500 ms) of **H8** (5 mM) and $\mathbf{OV}^{2+}\cdot(\mathbf{PF_6}^-)_2$ (5 mM) in DMSO-d_6/$CDCl_3$ (7/3, v/v) recorded at 45 °C reveal NOEs between (a) protons α and β of $\mathbf{OV}^{2+}$ and protons b2 through b8 of **H8**, (b) protons μ of $\mathbf{OV}^{2+}$ and protons b2 through b8 of **H8**, and (c) protons d and b2, and protons d and β. (d) Illustration of the 2 : 2 complex of **H8** and $\mathbf{OV}^{2+}$, with the major NOEs between the internal aromatic protons b1 through b8 of **H8** and protons α (shown in yellow) and β (shown in green) of $\mathbf{OV}^{2+}$ being indicated with double-headed arrows.

the two groups of otherwise equivalent aromatic protons of OV^{2+} give four discrete ^{1}H NMR peaks, suggesting that the two OV^{2+} ions in the cavity of **H16** are desymmetrized. Likewise, protons μ, *i.e.*, those of the methylene groups directly attached to the N^+ atoms of OV^{2+}, also give multiple signals. Assisted by COSY and NOESY spectra, the aromatic protons of OV^{2+} corresponding to the four ^{1}H NMR signals are labeled as α, β, γ, and δ. Four ^{1}H resonances can be attributed to methylene protons μ of OV^{2+}, which is due to the desymmetrization of the bound OV^{2+} ions and the methylene protons being diastereotopic in a helical cavity. The methylene protons corresponding to these four resonances are labeled as μ1, μ1′, μ2, and μ2′. The two halves of the desymmetrized OV^{2+} ion are defined by protons α, β, and μ1/μ1′, and protons γ, δ and μ2/μ2′, respectively.

The NOESY spectrum of **H16** and OV^{2+} (1 : 2) recorded in DMSO-d_6/$CDCl_3$ (4/6, v/v) at 45 °C reveals different NOEs between aromatic protons b1 (Fig. S9†), b2 through b16 of **H16** and protons α, δ (Fig. 7a), β, γ (Fig. 7b), and μ1/μ1′, μ2/μ2′ (Fig. 7c) of OV^{2+}. Strong NOEs are found between protons α and protons b2, b3, b4, b5, b6, and b7 (Fig. 7a) and b1 (Fig. S9†) that belong to the N-terminal half of **H16**. The intensities of NOEs involving protons α and protons b8 to b14 follow a descending order, with no NOEs being detected between protons α and protons b15 or b16. Compared to protons α, protons δ exhibit the opposite trend in the strength of their NOEs with aromatic protons b1–b16 of **H16** (Fig. 7a). Strong NOEs are found between protons δ and protons b9 through b16 that belong to the C-terminal half of **H16**, with NOEs involving protons δ decreasing consecutively from protons b8 to b3, and disappearing with protons b2 (Fig. 7a) and b1 (Fig. S9†). The NOEs observed between protons α and δ of OV^{2+}, and protons b1 through b16, along with the absence of NOE between the aromatic protons of OV^{2+} and protons c1–c16 of **H16** suggest that, similar to what is revealed by the crystal structure of complex **H16**·$(OV^{2+})_2$, in solution, the two OV^{2+} ions are aligned along the long axis of the cylindrical cavity of helix **H16**.

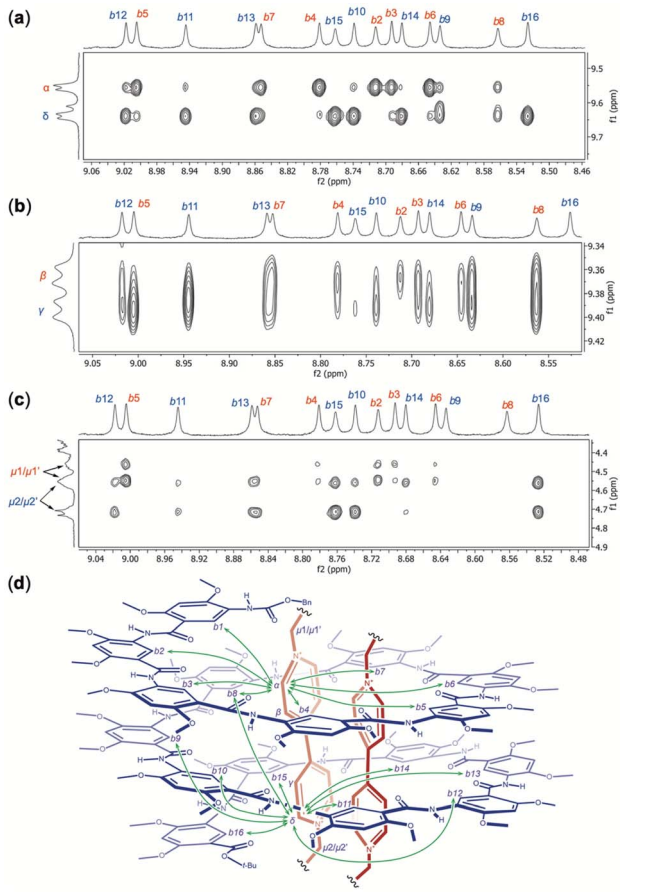

Fig. 7 Partial NOESY spectra (500 MHz, mixing time: 500 ms) of **H16** (3 mM) and OV^{2+}·$(PF_6^-)_2$ (6 mM) recorded in DMSO-d_6:$CDCl_3$ (4/6, v/v) at 45 °C reveal NOEs between protons b2 through b16 of **H16** and protons (a) α and δ, (b) β or γ, and (c) μ1/μ1′ and μ2/μ2′ of OV^{2+}. (d) Illustration of the 1 : 2 complex of **H16** and OV^{2+}, with the major NOEs between the internal aromatic protons b1 through b16 of **H16** and protons α and δ of OV^{2+} being indicated with double-headed arrows.

In addition to NOEs between the aromatic protons of guests OV^{2+} and those of **H16**, methylene protons μ also show NOE contacts that corroborate the solution structure of complex **H16**·$(OV^{2+})_2$. Protons μ1/μ1′ have obvious NOE contacts with protons b1 (Fig. S9†) and b2–b7 (Fig. 7c), while NOEs between protons μ2/μ2′ and protons b10–b16 are noticeable (Fig. 7c), which indicate that protons μ1/μ1′ and μ2/μ2′ are placed near the N- and C-termini of **H16**, respectively.

Therefore, the two ends of the OV^{2+} ion, as represented by protons α and μ1/μ1′, and δ and μ2/μ2′, are placed near the N- and C-termini, respectively, of **H16**. In such a complex, protons β and γ of OV^{2+} must be placed near the middle of helix **H16**. Indeed, protons β and γ have NOE contacts of similar strength with the most internal aromatic protons b of **H16** (Fig. 7b). The absence of NOE between protons β and protons b15 and b16, and between protons γ and protons b2 and b16 (Fig. 7b) provides additional evidence supporting the alignment of the OV^{2+} ions in the cavity of helix **H16** in solution (Fig. 7d).

The NOESY spectrum clearly demonstrates the binding of **H16** and guest TB^{2+} (Fig. S10†). Strong NOEs between protons b1 through b16 of **H16**, and aromatic protons α and methylene protons μ of TB^{2+} are detected, confirming that the cationic guest resides in the cavity of **H16**.

Conclusions

Aromatic oligoamides **H8** and **H16** fold into hollow helices with rigid (yet capable of slight induced-fit adjustments) electronegative cavities that strongly bind rodlike dicationic guests OV^{2+} and TB^{2+}. The 8-residue **H8**, a helix of ~1.2 turns, assembles into double helix $(H8)_2$ with a cavity capable of accommodating two OV^{2+} ions that align in an offset fashion. The resultant 2 : 2 complex, $(H8)_2$·$(OV^{2+})_2$ undergoes rapid exchange with the unbound host and guest. The 16-residue **H16**, which can be regarded as a covalent dimer of **H8**, serves as a unimolecular host with a 3D cavity that strongly binds guest OV^{2+}. The high stabilities of the resultant 1 : 1 complex **H16**·OV^{2+} and 1 : 2 complex **H16**·$(OV^{2+})_2$ are reflected by the slow exchange on the ^{1}H NMR time scale between the complexes and the unbound host and guest. The strong binding of **H16** for OV^{2+} is confirmed by ITC. The extraordinary affinity of **H16** for the first OV^{2+} ion and much weaker yet

significant binding for the second OV^{2+} ion point to highly negative cooperativity. In contrast, helix **H16** binds only one bulky guest TB^{2+} with the same affinity as that of **H16** with the first OV^{2+} ion, indicating that binding stoichiometry can be adjusted by tuning the structure (bulkiness) of the guest.

X-ray crystallography provides atomic details for complexes $(H8)_2\cdot(OV^{2+})_2$ and $H16\cdot(OV^{2+})_2$, which reveals the mutual adaption of the helical hosts and the dimeric guest. Double helix $(H8)_2$ provides a cavity that fully accommodates the two OV^{2+} ions. The crystal structure of complex $H16\cdot(OV^{2+})_2$ reveals that the two bound OV^{2+} ions undergo more compact alignment than those in $(H8)_2\cdot(OV^{2+})_2$, perhaps to better match the cavity of helix **H16**. In comparison to that of helix **H16** alone, the cavity of **H16** in complex $H16\cdot(OV^{2+})_2$ is slightly enlarged to better accommodate the two OV^{2+} ions.

In solution, the binding of OV^{2+} ions in the cavity of double helix $(H8)_2$ or helix **H16**, the head-on alignment of **H8** in duplex $(H8)_2$, and the desymmetrization of the otherwise symmetrical guest OV^{2+} in the cavity of **H16** are clearly demonstrated by two-dimensional (NOESY) ^{1}H NMR spectra. The binding of **H16** and guest TB^{2+} in solution is also been confirmed by the NOESY spectrum.

Complexes $(H8)_2\cdot(OV^{2+})_2$, $H16\cdot(OV^{2+})_2$ and $H16\cdot TB^{2+}$ are hitherto unknown double and single helical, [2]-, [3]-, and [4] pseudo-foldaxanes[40] featuring two and one axle components, respectively, with exceptional stabilities and a high degree of sophistication found with few rotaxanes and pseudo-rotaxanes. The observed tunability in binding stoichiometry is unusual among host–guest complexes. The presence of the discrete complex $H16\cdot(OV^{2+})_2$ demonstrates that hollow helices, as high-affinity hosts with 3D binding pockets, lead to host–guest complexes with significantly enhanced stability. The selective binding of **H16** for the OV^{2+} ion indicates that this host is capable of achieving optimum interactions despite the entropically unfavorable nature of the complexation. The resultant pseudo-foldaxanes, with foldaxane-like stability, are formed by simple mixing of the molecular components. By being able to tailor the size (length) and/or shape of guests, hollow helices, with their ready synthetic tunability, are new hosts that are uniquely different from hosts based on most macrocycles, resulting in host–guest complexes with adjustable sizes, stability, and binding stoichiometry. A largely unexplored aspect of our hollow helices involves the inherent chirality of these molecules. Resolving the racemic helices into optically pure left- and right-handed helices will also open a wide door allowing the exploration of a variety of chiral molecular recognition and transport processes.

Data availability

All relevant data supporting this article have been included in the main text and the ESI.†

Author contributions

Y. L. Z. and T. A. S. performed the major part of the experimental work including NMR data collection and ITC measurements, along with data analysis. Y. L. Z., B. S. and X. P. L. performed mass spectral studies. B. K. and Y. F. performed crystal growth, X-ray data collection, and crystal structure elucidation and refinement. B. G. conceptualised and supervised the study. I. H. contributed to the X-ray study and helped revise the manuscript. B. G. and Y. L. Z. wrote the manuscript. All authors commented on the data and reviewed the manuscript.

Conflicts of interest

There are no conflicts to declare.

Acknowledgements

We acknowledge support from the US National Science Foundation (CHE-1905094 and 2108538 to B. G.).

Notes and references

1 (*a*) J. M. Lehn, *Supramolecular Chemistry: Concepts and Perspectives*, VCH, Weinheim, 1995; (*b*) K. N. Houk, A. G. Leach, S. P. Kim and X. Zhang, *Angew. Chem., Int. Ed.*, 2003, **42**, 4872–4897.

2 (*a*) C. J. Pedersen and H. K. Frensdorff, *Angew. Chem., Int. Ed. Engl.*, 1972, **11**, 16–25; (*b*) G. A. Melson, *Coordination Chemistry of Macrocyclic Compounds*, Plenum Press, New York, 1979; (*c*) J. M. Lehn, *Supramolecular Chemistry: Concepts and Perspectives*, VCH, Weinheim, 1995.

3 B. Dietrich, in *Comprehensive Supramolecular Chemistry*, ed. G. W. Gokel, Elsevier, Oxford, 1999, vol. 1, pp. 153–211.

4 (*a*) D. J. Cram, *Science*, 1983, **219**, 1177–1183; (*b*) A. Wishard and B. C. Gibb, *Calixarenes and Beyond*, 2016, pp. 195–234.

5 (*a*) L. R. MacGillivray and J. L. Atwood, *Angew. Chem., Int. Ed.*, 1999, **38**, 1018–1033; (*b*) D. Fujita, K. Suzuki, S. Sato, M. Yagi-Utsumi, Y. Yamaguchi, N. Mizuno, T. Kumasaka, M. Takata, M. Noda, S. Uchiyama, K. Kato and M. Fujita, *Nat. Commun.*, 2012, **3**, 1093.

6 R. Breslow and S. D. Dong, *Chem. Rev.*, 1998, **98**, 1997–2012.

7 C. D. Gutsche, *Calixarenes*, Royal Society of Chemistry, Cambridge, 1989.

8 J. Lagona, P. Mukhopadhyay, S. Chakrabarti and L. Isaacs, *Angew. Chem., Int. Ed.*, 2005, **44**, 4844–4870.

9 M. Xue, Y. Yang, X. Chi, Z. Zhang and F. Huang, *Acc. Chem. Res.*, 2012, **45**, 1294–1308.

10 (*a*) K. Yazaki, L. Catti and M. Yoshizawa, *Chem. Commun.*, 2018, **54**, 3195–3206; (*b*) P. C. Kearney, L. S. Mizoue, R. A. Kumpf, J. E. Forman, A. McCurdy and D. A. Dougherty, *J. Am. Chem. Soc.*, 1993, **115**, 9907–9919; (*c*) Y.-X. Wang, Y.-M. Zhang, Y.-L. Wang and Y. Liu, *Chem. Mater.*, 2015, **27**, 2848–2854; (*d*) Y.-J. Ghang, J. J. Lloyd, M. P. Moehlig, J. K. Arguelles, M. Mettry, X. Zhang, R. R. Julian, Q. Cheng and R. J. Hooley, *Langmuir*, 2014, **30**, 10161–10166; (*e*) W. Liu, E. M. Peck, K. D. Hendzel and B. D. Smith, *Org. Lett.*, 2015, **17**, 5268–5271.

11 K. Ariga and T. Kunitake, *Supramolecular Chemistry—Fundamentals and Applications*. Springer, New York, 2006.

12 M. V Rekharsky, T. Mori, C. Yang, Y. H. Ko, N. Selvapalam, H. Kim, D. Sobransingh, A. E. Kaifer, S. Liu, L. Isaacs,

W. Chen, S. Moghaddam, M. K. Gilson, K. Kim and Y. Inoue, *Proc. Natl. Acad. Sci.*, 2007, **104**, 20737–20742.
13 R. B. Schoch, J. Han and P. Renaud, *Rev. Mod. Phys.*, 2008, **80**, 839–883.
14 B. Hinds, *Curr. Opin. Solid State Mater. Sci.*, 2012, **16**, 1–9.
15 (*a*) D. T. Bong, T. D. Clark, J. R. Granja and M. R. Ghadiri, *Angew. Chem., Int. Ed.*, 2001, **40**, 988–1011; (*b*) W. S. Childers, R. Ni, A. K. Mehta and D. G. Lynn, *Curr. Opin. Chem. Biol.*, 2009, **13**, 652–659; (*c*) B. Gong and Z. Shao, *Acc. Chem. Res.*, 2013, **46**, 2856–2866; (*d*) L. S. Shimizu, S. R. Salpage and A. A. Korous, *Acc. Chem. Res.*, 2014, **47**, 2116–2127; (*e*) A. Ghorai, B. Achari and P. Chattopadhyay, *Tetrahedron*, 2016, **72**, 3379–3387; (*f*) A. Nitti, A. Pacini and D. Pasini, *Nanomaterials*, 2017, **7**, 167.
16 M. A. B. Block, C. Kaiser, A. Khan and S. Hecht, *Top. Curr. Chem.*, 2005, **245**, 89–150.
17 J. G. Moralez, J. Raez, T. Yamazaki, R. K. Motkuri, A. Kovalenko and H. Fenniri, *J. Am. Chem. Soc.*, 2005, **127**, 8307–8309.
18 P. Jonkheijm, A. Miura, M. Zdanowska, F. J. M. Hoeben, S. De Feyter, A. P. H. J. Schenning, F. C. De Schryver and E. W. Meijer, *Angew. Chem., Int. Ed.*, 2004, **43**, 74–78.
19 (*a*) D. L. Gin, W. Gu, B. A. Pindzola and W.-J. Zhou, *Acc. Chem. Res.*, 2001, **34**, 973–980; (*b*) M. Zhou, P. R. Nemade, X. Lu, X. Zeng, E. S. Hatakeyama, R. D. Noble and D. L. Gin, *J. Am. Chem. Soc.*, 2007, **129**, 9574–9575.
20 V. Percec, A. E. Dulcey, V. S. K. Balagurusamy, Y. Miura, J. Smidrkal, M. Peterca, S. Nummelin, U. Edlund, S. D. Hudson, P. A. Heiney, H. Duan, S. N. Magonov and S. A. Vinogradov, *Nature*, 2004, **430**, 764–768.
21 J. M. Schnur, *Science*, 1993, **262**, 1669–1676.
22 B. Gong, *Chem.–Eur. J.*, 2001, **7**, 4336–4342.
23 V. Berl, M. J. Krische, I. Huc, J.-M. Lehn and M. Schmutz, *Chem.–Eur. J.*, 2000, **6**, 1938–1946.
24 (*a*) J. C. Nelson, J. G. Saven, J. S. Moore and P. G. Wolynes, *Science*, 1997, **277**, 1793–1796; (*b*) R. B. Prince, S. A. Barnes and J. S. Moore, *J. Am. Chem. Soc.*, 2000, **122**, 2758–2762.
25 H. Abe, N. Masuda, M. Waki and M. Inouye, *J. Am. Chem. Soc.*, 2005, **127**, 16189–16196.
26 J.-L. Hou, X.-B. Shao, G.-J. Chen, Y.-X. Zhou, X.-K. Jiang and Z.-T. Li, *J. Am. Chem. Soc.*, 2004, **126**, 12386–12394.
27 (*a*) J. Garric, J.-M. Léger and I. Huc, *Angew. Chem., Int. Ed.*, 2005, **44**, 1954–1958; (*b*) C. Bao, B. Kauffmann, Q. Gan, K. Srinivas, H. Jiang and I. Huc, *Angew. Chem., Int. Ed.*, 2008, **47**, 4153–4156; (*c*) P. Mateus, B. Wicher, Y. Ferrand and I. Huc, *Chem. Commun.*, 2018, **54**, 5078–5081.
28 J. Y. Hwang, H.-G. Jeon, Y. R. Choi, J. Kim, P. Kang, S. Lee and K.-S. Jeong, *Org. Lett.*, 2017, **19**, 5625–5628.
29 A.-M. Stadler, N. Kyritsakas and J.-M. Lehn, *Chem. Commun.*, 2004, 2024–2025.
30 J.-L. Hou, M.-X. Jia, X.-K. Jiang, Z.-T. Li and G.-J. Chen, *J. Org. Chem.*, 2004, **69**, 6228–6237.
31 F. Zhang, S. Bai, G. P. A. Yap, V. Tarwade and J. M. Fox, *J. Am. Chem. Soc.*, 2005, **127**, 10590–10599.
32 K. Yamato, L. Yuan, W. Feng, A. J. Helsel, A. R. Sanford, J. Zhu, J. Deng, X. C. Zeng and B. Gong, *Org. Biomol. Chem.*, 2009, **7**, 3643–3647.
33 J. Shen, C. Ren and H. Zeng, *J. Am. Chem. Soc.*, 2017, **139**, 5387–5396.
34 (*a*) K.-J. Chang, B.-N. Kang, M.-H. Lee and K.-S. Jeong, *J. Am. Chem. Soc.*, 2005, **127**, 12214–12215; (*b*) J. Suk and K.-S. Jeong, *J. Am. Chem. Soc.*, 2008, **130**, 11868–11869.
35 H. Juwarker, J. M. Lenhardt, D. M. Pham and S. L. Craig, *Angew. Chem., Int. Ed.*, 2008, **47**, 3740–3743.
36 Y. Hua, Y. Liu, C.-H. Chen and A. H. Flood, *J. Am. Chem. Soc.*, 2013, **135**, 14401–14412.
37 V. Diemer, L. Fischer, B. Kauffmann and G. Guichard, *Chem.–Eur. J.*, 2016, **22**, 15684–15692.
38 (*a*) C. J. Massena, N. B. Wageling, D. A. Decato, E. Martin Rodriguez, A. M. Rose and O. B. Berryman, *Angew. Chem., Int. Ed.*, 2016, **55**, 12398–12402; (*b*) E. A. John, C. J. Massena and O. B. Berryman, *Chem. Rev.*, 2020, **120**, 2759–2782.
39 R. Cao, R. B. Rossdeutcher, B. Gong and X. Wu, *Org. Lett.*, 2020, **22**, 7496–7501.
40 V. Koehler, A. Roy, I. Huc and Y. Ferrand, *Acc. Chem. Res.*, 2022, **55**, 1074–1085.
41 R. Suresh, N. Venkataraman, S. Vasudevan and K. V Ramanathan, *J. Phys. Chem. C*, 2007, **111**, 495–500.
42 N. Chandramouli, Y. Ferrand, G. Lautrette, M. Laguerre, I. Huc, B. Kauffmann, C. D. Mackereth and D. Dubreuil, *Nat. Chem.*, 2015, **7**, 334–341.
43 R. D. Parra, H. Zeng, J. Zhu, C. Zheng, X. C. Zeng and B. Gong, *Chem.–Eur. J.*, 2001, **7**, 4352–4357.
44 (*a*) B. Gong, *Acc. Chem. Res.*, 2008, **41**, 1376–1386; (*b*) J. Zhu, R. D. Parra, H. Zeng, E. Skrzypczak-Jankun, X. C. Zeng and B. Gong, *J. Am. Chem. Soc.*, 2000, **122**, 4219–4220; (*c*) B. Gong, H. Zeng, J. Zhu, L. Yua, Y. Han, S. Cheng, M. Furukawa, R. D. Parra, A. Y. Kovalevsky, J. L. Mills, E. Skrzypczak-Jankun, S. Martinovic, R. D. Smith, C. Zheng, T. Szyperski and X. C. Zeng, *Proc. Natl. Acad. Sci.*, 2002, **99**, 11583–11588; (*d*) L. Yuan, H. Zeng, K. Yamato, A. R. Sanford, W. Feng, H. S. Atreya, D. K. Sukumaran, T. Szyperski and B. Gong, *J. Am. Chem. Soc.*, 2004, **126**, 16528–16537.
45 Y. Zhong, B. Kauffmann, W. Xu, Z.-L. Lu, Y. Ferrand, I. Huc, X. C. Zeng, R. Liu and B. Gong, *Org. Lett.*, 2020, **22**, 6938–6942.
46 T. A. Sobiech, Y. L. Zhong, L. S. Sánchez, B. Kauffmann, J. K. McGrath, C. Scalzo, D. P. Miller, I. Huc, E. Zurek, Y. Ferrand and B. Gong, *Chem. Commun.*, 2021, **57**, 11645–11648.
47 (*a*) C. A. Hunter and H. L. Anderson, *Angew. Chem., Int. Ed.*, 2009, **48**, 7488–7499; (*b*) L. K. S. von Krbek, C. A. Schalley and P. Thordarson, *Chem. Soc. Rev.*, 2017, **46**, 2622–2637.
48 (*a*) V. Berl, I. Huc, R. G. Khoury, M. J. Krische and J.-M. Lehn, *Nature*, 2000, **407**, 720–723; (*b*) C. Bao, Q. Gan, B. Kauffmann, H. Jiang and I. Huc, *Chem.–Eur. J.*, 2009, **15**, 11530–11536; (*c*) Y. Ferrand, Q. Gan, B. Kauffmann, H. Jiang and I. Huc, *Angew. Chem., Int. Ed.*, 2011, **50**, 7572–7575.
49 H.-J. Kim, J. Heo, W. S. Jeon, E. Lee, J. Kim, S. Sakamoto, K. Yamaguchi and K. Kim, *Angew. Chem., Int. Ed.*, 2001, **40**, 1526–1529.
50 J.-M. Zhao, Q.-S. Zong, T. Han, J.-F. Xiang and C.-F. Chen, *J. Org. Chem.*, 2008, **73**, 6800–6806.